Toxicologic Pathology, 32(Suppl. 1):1–9, 2004

ISSN: 0192-6233 print / 1533-1601 online
DOI: 10.1080/01926230490426516

Toxicoproteomics: Serum Proteomic Pattern Diagnostics for Early Detection of Drug Induced Cardiac Toxicities and Cardioprotection

EMANUEL F. PETRICOIN,[1] VINODH RAJAPASKE,[2] EUGENE H. HERMAN,[3] ALI M. AREKANI,[1] SALLY ROSS,[2] DONALD JOHANN,[2] ALAN KNAPTON,[3] J. ZHANG,[3] BEN A. HITT,[4] THOMAS P. CONRADS,[5] TIMOTHY D. VEENSTRA,[5] LANCE A. LIOTTA,[2] AND FRANK D. SISTARE[3]

[1]*FDA-NCI Clinical Proteomics Program, Office of Cell and Gene Therapies, Center for Biologic Evaluation and Research, Food and Drug Administration, Bethesda, Maryland, USA*
[2]*FDA-NCI Clinical Proteomics Program, Laboratory of Pathology, Center for Cancer Research, NCI, NIH, Bethesda, Maryland, USA*
[3]*Division of Applied Pharmacology Research, Center for Drug Evaluation and Research, Food and Drug Administration, Laurel, Maryland, USA*
[4]*Correlogic Systems, Inc., Bethesda, Maryland, USA, and*
[5]*NCI Biomedical Proteomics Program, Analytical Chemistry Laboratory, Mass Spectrometry Center, SAIC Frederick, Inc., SAIC-NCI, Frederick, Maryland, USA*

QUERY SHEET

Q1: Au: Please provide 6-8 keywords for this article.
Q2: Au: Please provide year.
Q3: Au: Need year here and in text.
Q4: Au: Need year here and in text.
Q5: Au: Please list all authors for this article.
Q6: Au: Please list all authors for the article.
Q7: Au: Need page range here.

Toxicologic Pathology, 32(Suppl. 1):1–9, 2004

ISSN: 0192-6233 print / 1533-1601 online
DOI: 10.1080/01926230490426516

Toxicoproteomics: Serum Proteomic Pattern Diagnostics for Early Detection of Drug Induced Cardiac Toxicities and Cardioprotection

EMANUEL F. PETRICOIN,[1] VINODH RAJAPASKE,[2] EUGENE H. HERMAN,[3] ALI M. AREKANI,[1] SALLY ROSS,[2] DONALD JOHANN,[2] ALAN KNAPTON,[3] J. ZHANG,[3] BEN A. HITT,[4] THOMAS P. CONRADS,[5] TIMOTHY D. VEENSTRA,[5] LANCE A. LIOTTA,[2] AND FRANK D. SISTARE[3]

[1]*FDA-NCI Clinical Proteomics Program, Office of Cell and Gene Therapies, Center for Biologic Evaluation and Research, Food and Drug Administration, Bethesda, Maryland, USA*
[2]*FDA-NCI Clinical Proteomics Program, Laboratory of Pathology, Center for Cancer Research, NCI, NIH, Bethesda, Maryland, USA*
[3]*Division of Applied Pharmacology Research, Center for Drug Evaluation and Research, Food and Drug Administration, Laurel, Maryland, USA*
[4]*Correlogic Systems, Inc., Bethesda, Maryland, USA, and*
[5]*NCI Biomedical Proteomics Program, Analytical Chemistry Laboratory, Mass Spectrometry Center, SAIC Frederick, Inc., SAIC-NCI, Frederick, Maryland, USA*

ABSTRACT

Proteomics is more than just generating lists of proteins that increase or decrease in expression as a cause or consequence of pathology. The goal should be to characterize the information flow through the intercellular protein circuitry which communicates with the extracellular microenvironment and then ultimately to the serum/plasma macroenvironment. The nature of this information can be a cause, or a consequence, of disease and toxicity based processes as cascades of reinforcing information percolate through the system and become reflected in changing proteomic information content of the circulation. Serum Proteomic Pattern Diagnostics is a new type of proteomic platform in which patterns of proteomic signatures from high dimensional mass spectrometry data are used as a diagnostic classifier. While this approach has shown tremendous promise in early detection of cancers, detection of drug-induced toxicity may also be possible with this same technology. Analysis of serum from rat models of anthracycline and anthracenedione induced cardiotoxicity indicate the potential clinical utility of diagnostic proteomic patterns where low molecular weight peptides and protein fragments may have higher accuracy than traditional biomarkers of cardiotoxicity such as troponins. These fragments may one day be harvested by circulating nanoparticles designed to absorb, enrich and amplify the diagnostic biomarker repertoire generated even at the critical initial stages of toxicity.

Keywords.

TOXICOPROTEOMICS

Despite the urgent clinical need to discover serum biomarkers for the early detection of disease and drug induced toxicity, the number of new biomarkers reaching routine clinical use remains unacceptably low (Ward and Henderson, 1996; Anderson and Anderson, 2002). The low molecular mass range (<15,000 Daltons) of the serum proteome, while until most recently was largely uncharacterized, promises to contain a rich source of previously undiscovered biomarkers (Tirumalai et al., 2003) as the biological processes give rise to cascades of enzymatically generated and proteolytically clipped biomarker fragments. The blood proteome is changing constantly as a consequence of the perfusion of the organ undergoing drug-induced damage and this process then adds, subtracts, or modifies the circulating proteome. Thus, even if these small peptide fragments are many degrees of separation removed from the actual insult, they can retain the specificity for the disease because this process can arise from a specific type of biomarker amplification based on the uniqueness of the tissue microenvironment where the organ toxicity occurs. These low molecular mass molecules exist below the range of detection achieved by conventional 2-D gel electrophoresis since they cannot be efficiently separated by gel-based techniques (Tirumalai et al., 2003). Consequently, investigators have turned to mass spectroscopy, which exhibits optimal performance in the low mass range (Kantor, 2002; McDonald and Yates, 2002).

Under the assumption that the low molecular mass biomarkers contain important diagnostic information, the search for low mass serum/plasma biomarkers usually begins with a separation step to remove the abundant high molecular mass "contaminating" proteins such as albumin, thyroglobulin, and immunoglobulins so that the analysis can be focused on the lower molecular mass region. However, from a physiologic perspective, discarding higher molecular weight and abundant proteins may be an incorrect means for optimal biomarker discovery. Free phase low molecular weight molecules should be rapidly cleared through the kidney, significantly reducing the concentration of these potential biomarkers to a level below detection of any clinical testing device. However, in the face of the vast excess of high molecular weight serum proteins, it may be likely that low abundance and low mass biomarkers will tend to become bound to large high abundant carrier proteins and protected from kidney clearance (Maack, 1975; Cojocel et al., 1984).

Address correspondence to: Emanuel F. Petricoin, FDA-NCI Clinical Proteomics Program, Building 29A Room 2D12, 8800 Rockville Pike, Bethesda, Maryland 20892, USA; e-mail: petricoin@cber.fda.gov

Thus the half-life of bound low abundance and low molecular weight carrier proteins possess a half-life that is many orders of magnitude longer than the free-phase small molecules. Circulating carrier proteins have been recently found to act as a reservoir for the accumulation and amplification of bound low mass biomarkers, integrating, amplifying and storing diagnostic information like a capacitor stores electricity (Liotta et al., 2003; Mehta et al., 2003).

To be clinically useful, a toxicity-related biomarker should be measurable in an accessible body fluid such as serum, urine or saliva. Because these body fluids are a protein-rich information reservoir that contains the traces of what the blood has encountered on its constant perfusion and percolation throughout the body, proteomics may offer the best chance of discovering these early stage changes. In the past, the search for early disease and toxicity biomarkers has been a methodical and laborious approach that included the search for over expressed proteins in blood that were shed into the circulation as a consequence of a disease process. There are potentially thousands of intact and cleaved proteins in the human serum proteome, so finding the single disease-related protein could be like searching for a needle in a haystack, requiring the separation and identification of each protein biomarker.

Initial studies employing mass spectroscopy for the identification of biomarker patterns for cancer diagnosis and classification have been very promising (Adam et al., 2002; Li et al., 2002; Petricoin et al., 2002a, 2002b, 2002c; Conrads et al., 2003; Hingorani et al., 2003; Petricoin and Liotta, 2003a, 2003b). Unlike past attempts that start with a known single marker candidate, proteomic pattern analysis begins with high-dimensional data, usually produced by high-throughput mass spectrometry. This diagnostic method seeks, without bias, to identify patterns of low molecular weight biomarkers as ion peak features within the spectra, and use these patterns as the diagnostic endpoint itself.

Serum Proteomic Pattern Diagnostics: Producing the Mass Spectra

While investigators have used a variety of different bioinformatic algorithms for pattern discovery, the most common analytical platform is comprised of a Protein Chip Biomarker System-II [PBS-II, a low-resolution time-of-flight (TOF) mass spectrometer (MS)]. Herein samples are ionized by surface enhanced laser desorption/ionization (SELDI), a Protein Chip array-based chromatographic retention technology that allows for direct mass spectrometric analysis of analytes retained on the array (Figure 1). Only a subset of the proteins in the serum bind to the chromatographic surface of the chip, and the unbound proteins are washed away. The adherent proteins are treated with acid (so that they can become ionized) and then dried down onto the surface. The bait region containing individual captured serum protein samples, dried down on a row of spots, is inserted into a vacuum chamber and a laser beam is fired at each spot. The laser energy blasts off (desorbs) the ionized proteins, and the ionized proteins fly down the vacuum tube toward an oppositely charged electrode. The mass to charge value of each ion is estimated from the time it takes for the launched ion to reach the electrode; small ions travel faster. Therefore, the spectrum provides a "time of flight" (TOF) signature of ions ordered by size. Recently this concept has been extended to a high-resolution MS as it has been found that higher resolution MS data generates diagnostic models possessing higher sensitivities and specificities as a result of the increased number of peaks seen and the much better between and within machine reproducibility (Conrads et al., 2003). Moreover, the spectral resolution of the lower resolution instrumentation cannot separate specific ions that are close in mass/charge and which can coalesce multiple specific discreet ions into a single peak. The high-resolution mass spectrometer used in our studies is a hybrid quadrupole time-of-flight mass spectrometer (QSTAR pulsar *i*, Applied Biosystems Inc., Framingham, Massachusetts) fitted with a ProteinChip array interface (Ciphergen Biosystems Inc.) and externally calibrated twice a day using a mixture of known peptides. As a point of analytical comparison, the Qq-TOF MS (routine resolution ~8,000) can completely resolve species differing in m/z of only 0.375 (e.g., at m/z 3000) whereas complete resolution of species with the PBS-II TOF MS (routine resolution ~150) is only possible for species that differ by m/z of 20 (Figure 2).

In a clinical setting where a pattern test may be eventually employed as a diagnostic, it will be important to determine overall spectral quality and develop spectral release specifications such that variances introduced into the process can be evaluated and monitored. Day-to-day, lot-to-lot, and machine-to-machine variances brought in from sample handling/storage and shipping conditions will need to be evaluated and understood as well as the mass spectrometer itself. To that end, we employ a pooled reference standard sample, obtained from NIST (SRM-1951A) which is randomly applied to one spot on each protein array as a quality control for overall process integrity, sample preparation and mass spectrometer function. Additionally, for spectral quality control, quality assurance and spectral release specification, all spectra are subjected to plotting by total ion current (total record count), average/mean and standard deviation of amplitude, chi-square, and *t*-test analysis of each ion or bin, and quartile plotting measures using JMP (SAS Institute, Cary, NC) software as well as stored procedures that we developed in-house, prior to any pattern discovery. Process measures are checked by analyzing the statistical plots of the NIST serum reference standard, and spectra that fail statistical checks for homogeneity are eliminated from in-depth modeling and analysis. This type of upfront analysis is critical for comparing the total analytical variance obtained for the constant NIST reference sample with the variance of the clinical sample populations. The total variance of the reference sample should be no less than that for the clinical specimens.

ProteinChip arrays (Ciphergen Biosystems Inc) are typically processed in parallel using a Biomek Laboratory workstation (Beckman-Coulter) modified to make use of a ProteinChip array bioprocessor (Ciphergen Biosystems Inc.). The bioprocessor holds 12 ProteinChips, each having 8 chromatographic "spots," allowing 96 samples to be processed in parallel and matrix applied using a liquid robotic handling station (Genesis Freedom 200, TECAN; Research Triangle Park, NC).

Serum Proteomic Pattern Diagnostics: Uncovering the Pattern Classifiers

The proteomic pattern analysis is performed by first exporting the raw data file generated from the QSTAR mass

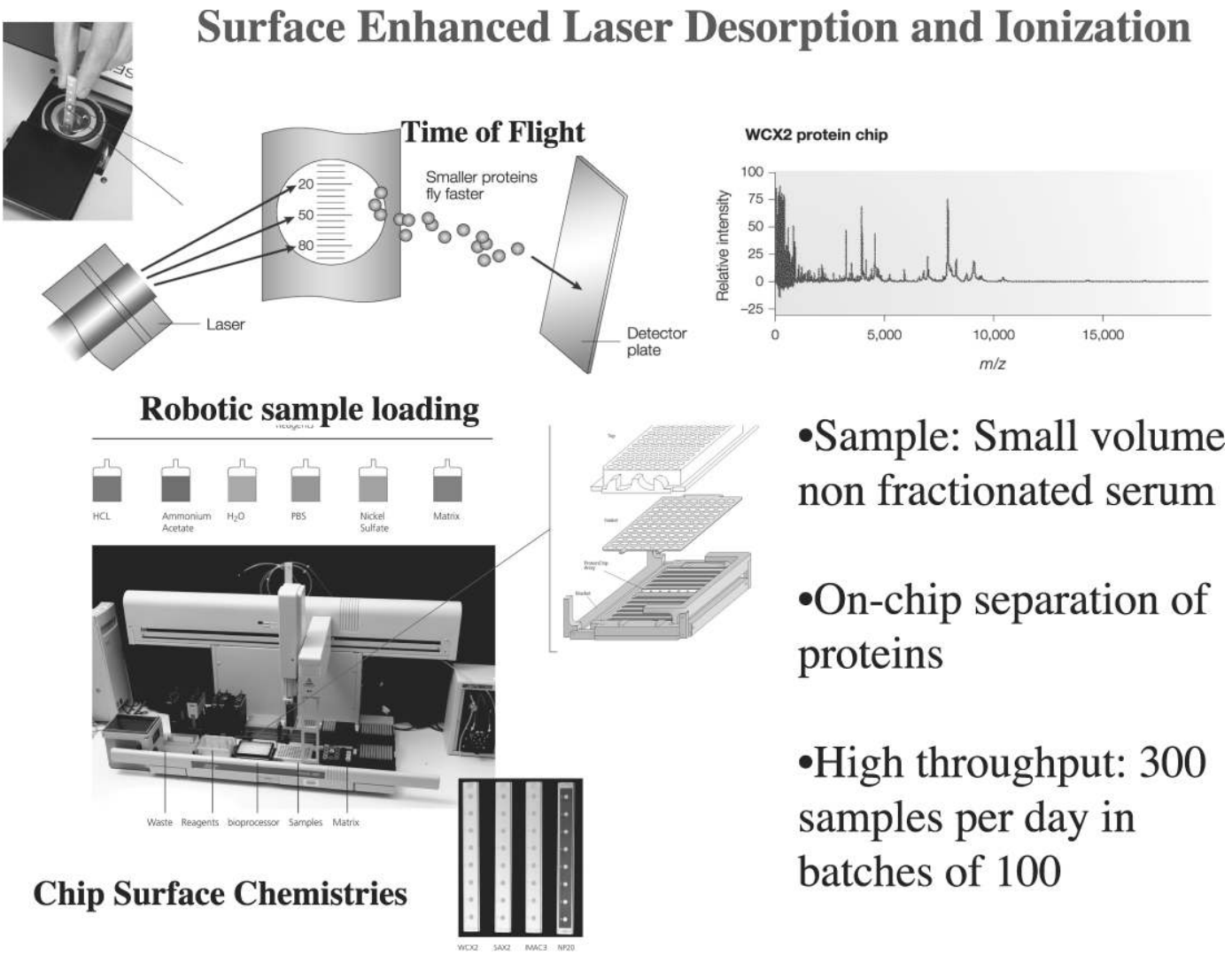

FIGURE 1.—Surface enhanced laser desorbtion and ionization (SELDI) technology. This type of proteomic analytical tool is a class of mass spectroscopy instrument useful in high throughput proteomic fingerprinting of serum. Using a robotic sample dispenser, 1 μL of serum is applied to the surface of a protein binding chip. A subset of the proteins in the sample bind to the surface of the chip. The bound proteins are treated with a MALDI matrix, washed and dried. The chip, containing multiple patient samples, is inserted into a vacuum chamber where it is irradiated with a laser. The laser desorbs the adherent proteins, causing them to be launched as ions. The time of flight (TOF) of the ion prior to detection by an electrode is a measure of the mass to charge (M/Z) value of the ion. The ion spectra can be analyzed by computer-assisted tools that classify a subset of the spectra by their characteristic patterns of relative intensity.

spectra into tab-delimited files that generated approximately 350,000 data points per spectrum. The high-resolution spectra is then binned using a function of 400 parts per million (ppm) such that all data files possess identical m/z values (e.g., the m/z bin sizes linearly increase from 0.28 at m/z 700 to 4.75 at m/z 12,000). This binning process actually condenses the number of data points from 350,000 to exactly 7,084 points per sample, and by a ppm binning function the m/z range of the bins gradually increases as a function of the resolution capacity of the machine. The 400 ppm binning function was based on a value obtained by a 10 times the estimate of what the mass drift of the Qq-TOF machine routinely obtains by external and internal calibration results (5–40 ppm)—as a conservative drift bracket.

The data are then randomly separated into equal groups for training, and testing with the models built on the training set using ProteomeQuest (Correlogic Systems Inc., Bethesda, Maryland) and tested using blinded sample sets. The m/z values in the models that were generated by the high-resolution instrument are based on the binned data and not the actual m/z values from the raw mass spectra. The Proteome Quest software itself implements a pattern discovery algorithm combining elements from genetic algorithms and self-organizing adaptive pattern recognition systems (Tou and Gonzalez, 1974; Kohonen, 1982, 1990; Holland, 1994). Genetic algorithms organize and analyze complex data sets as if they were information comprised of individual elements that can be manipulated through a computer-driven analog of a natural selection process. Self-organizing systems cluster data patterns into similar groups. Adaptive systems recognize novel events and track rare instances. The genetic algorithm component of the analysis begins with the random generation

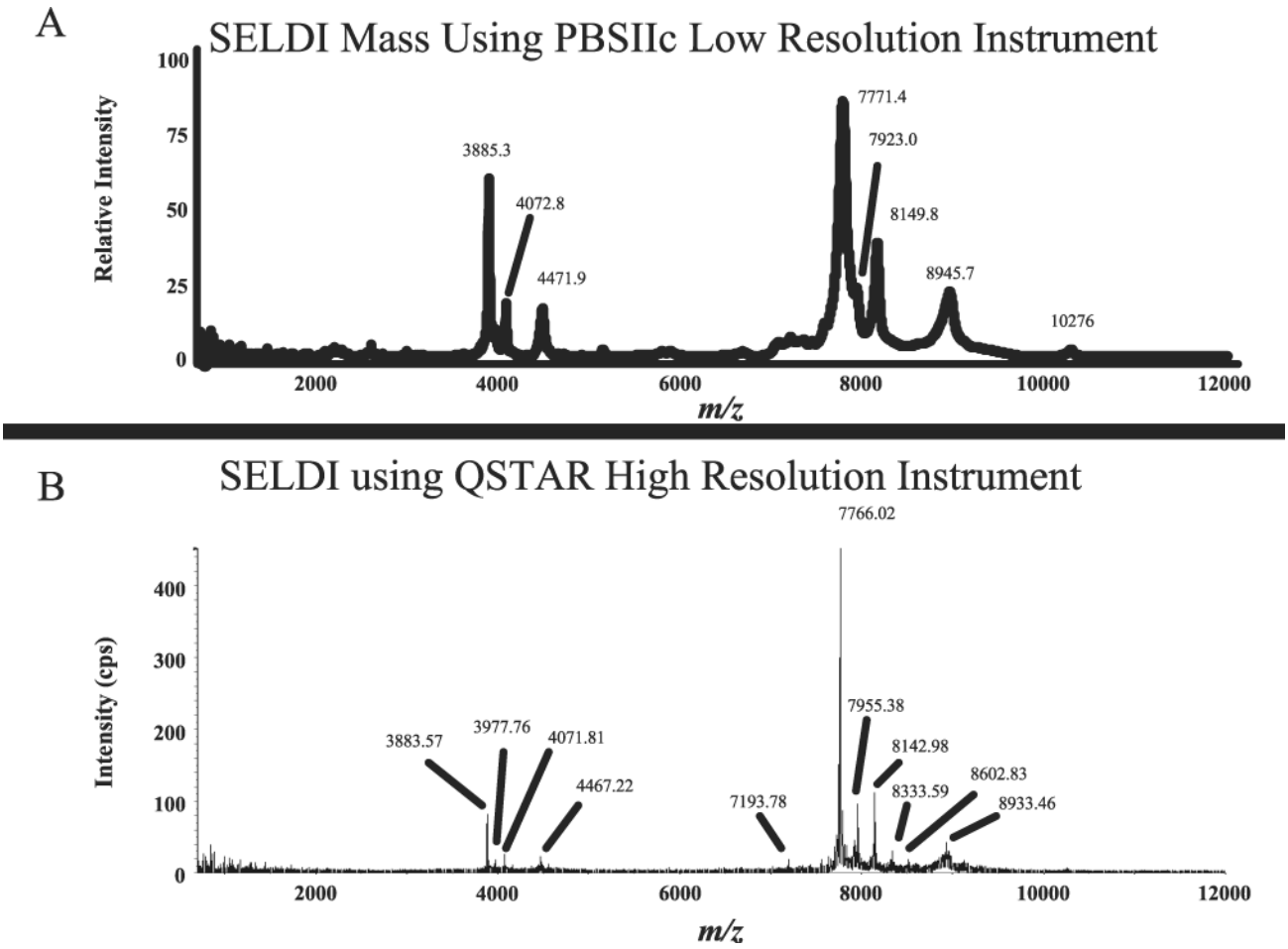

FIGURE 2.—Comparison between low resolution and high resolution SELDI-TOF mass spectra. Spectra from the same weak cation exchange chip (queried at the same spot) were generated on either a PBS IIc (Ciphergen Biosystems, Inc.) low resolution instrument (Panel A, top) or on a high resolution QSTAR pulsar *i*, (Applied Biosystems Inc., Framingham, Massachusetts) (Panel B, bottom).

of a population of 1,500 subsets, of combinations of ion features of the mass spectra. This number was chosen based on adequate coverage of the data, with a heuristic that no value can be duplicated within each of the 1,500 subsets. Each subset in the population specifies the identities of the exact M/Z values in each data stream but not their relative amplitude. The number of ion features in the subset ranges from 5 to 20.

Data normalization is an important element of pattern recognition as bias introduced by protein chip quality, mass spectrometer instrumentation and operator variance can effect overall spectral performance. Moreover, it is likely that different data normalization procedures will generate different ions selected, especially in a clustering algorithm where multiple ion features are used as the pattern. Since mass spectrometry is not inherently quantitative, scalar intensity changes may be apparent, yet the overall pattern may not be changed. One way we typically normalize mass spectral data is by dividing the amplitudes at each M/Z value within any randomly generated pattern subset by the largest value within that subset. In this way, differences in spectral quality that may emanate from biases such as in protein chip variance and not from the inherent disease process itself, can be minimized. Also, this method allows for low amplitude features to contribute substantially to the classification. The spectra are normalized according to the following formula:

$$\mathrm{NV} = (\mathrm{V} - \mathrm{Min})/(\mathrm{Max} - \mathrm{Min})$$

NV is the normalized value, V the intensity value for the specific randomly chosen m/z bin in question, Min the intensity of the smallest intensity value of any of the m/z bins within the randomly selected pattern and Max the maximum intensity of the m/z bin within the randomly selected pattern. This equation linearly normalizes the peak intensities so as to fall within the range of 0 to 1. Each of the randomly selected 1,500-subset patterns was then subjected to a fitness test.

The fitness test in these analyses is the ability of the combined ion amplitude values of any candidate subset to specify a lead cluster map that generates homogeneous clusters containing only diseased subjects or unaffected subjects used in the training sets. The lead cluster map is a self-organizing, adaptive pattern recognition algorithm that uses Euclidean distance to group vectors of data. The map begins as an empty N-dimensional space where N is the number of m/z features in the data vector. The optimal discriminatory pattern is identified by finding the best combination of m/z bins whose

normalized ion intensity values in *N*-dimensional space creates a unique identifier or cluster of identifiers. Any given training sample is compared for its proximity to previously defined clusters of diseased and unaffected subjects in *N*-space. If an *N*-dimensional identifier vector from a subject in the training group falls within the decision boundary of an existing cluster, then the subject is classified as belonging to that group. For these studies, the decision boundary is defined as 10% of maximum distance allowed in the space. This corresponds to a 90% pattern match. Thus, the decision boundary is referred to as the 90% boundary. If the data vector does not fall within the 90% decision boundary of any existing cluster in the model it is used to establish a new cluster and is identified as a new observation. The process is repeated once for each vector in the collection of training data.

Those subpopulation patterns that best discriminate the training set are more likely to survive the culling of the population to the original population size, e.g., 1,500, and contribute to the next generation of fit candidate patterns. The progeny of the most-fit patterns are generated through crossover and mutation of the 5–20 specific mass/charge bin values within each subset. Each subset is evaluated by its ability to accurately distinguish the two training set populations. As a result, each successive population of subsets is, on average, more fit than its predecessor. To ensure that the algorithms do not trend to less than near optimal decision points, a "mutation" rate is built into the process such that 0.02% of the m/z bin values are randomly rechosen. Crossover operations are of single point type and are randomly selected in each mating. For example, if there are 5 mass/charge bin values there can be 4 crossover points. The genetic algorithm is iterated for at least 250 generations or until a lead cluster map that homogeneously separates diseased from unaffected is generated. The lead cluster map that best separates diseased from unaffected is deployed for validation using blinded test sets.

Test data, not used during the training process, are then analyzed in the following steps. The data is normalized as described above and the normalized relative amplitudes of the test sample spectra at the *N* defined M/Z values bins are used to fix a point in N-dimensional space. The Euclidean distance vector is then calculated between this point and the center of all clusters (both cancer and unaffected) formed by the training set. If the unknown test vector falls inside the 90% boundary surrounding any centroid, then it is classified as being a member of that cluster and given a probability score based on its proximity to the theoretical center of the cluster and the number of records within that cluster. Otherwise, it is scored as a "new cluster." The results from the testing set of data are used for determination of sensitivity, specificity and positive predictive value of the patterns.

As each new patient is validated through pathological diagnosis using retrospective or prospective study sets, its input can be added to the ongoing clustering using the same models. The AI tool learns, adapts and gains experience through

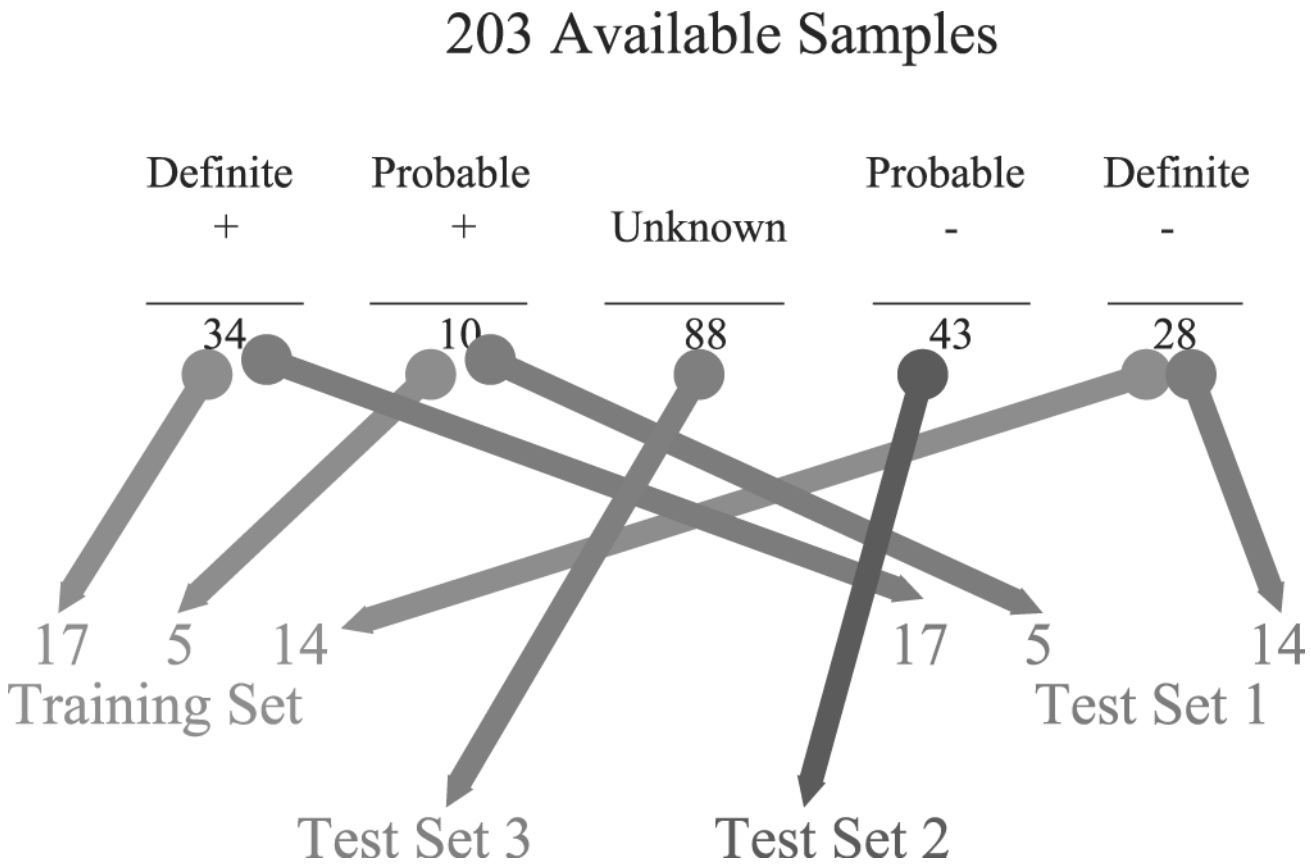

FIGURE 3.—Cardiotoxicity study set design for proteomic pattern diagnostics. A total of 203 specimens from SHR rats were used for training (N = 36, green) and testing (N = 36 testing set 1, red) from animals with acute doxorubicin cardiotoxicity, subacute, and saline alone controls. After the model comprised of 5 m/z features was found, separate challenge studies with two independent testing sets were used.

constant vigilant updating. In fact, it is possible to generate not just one, but multiple combinations of proteomic patterns from a single mass spectral training set, each pattern combination readjusting as the models get better in the adaptive mode.

DETECTION OF DOXORUBICIN INDUCED CARDIOTOXICITY USING SERUM PROTEOMIC PATTERN DIAGNOSTICS

Animal models that can portray and recapitulate mechanistically what may occur in the human are of vital importance for the drug development process. Toxicoproteomics can be utilized in this setting whereby serum proteomic biomarker patterns associated with known drug-induced toxicities can be matched against an experimental therapeutic under preclinical evaluation and predictive correlates obtained to guide and select which compounds should be taken forward or shelved. A drug/organ toxicity system that has been extensively characterized in both animals and human subjects is that of anthracycline induced cardiotoxicity (Alderton et al., (); Lambertenghi-Deliliers et al., 1976; Bristow et al., 1981; Zhang et al., 1993; Hasinoff et al., 1998; Herman and Ferrans, 1998; Ewer et al., 1999; Herman et al., 2001; Zhang et al., 2002). This study system has both well known pathological and serum biomarker endpoints (cardiac lesion histological changes and serum cardiac troponin concentrations, respectively) that have been used recently to measure effects of therapeutic compounds on cardiac damage. Using the Spontaneously Hypertensive Rat (SHR) model, in which animals were challenged with doxorubicin or with mitoxantone +/− dexrazoxane (a routinely used cardioprotectant), over 200 samples collected and stored frozen over a 4-year period (N = 203) were analyzed to evaluate whether high-resolution serum proteomic patterns could outperform serum cardiac troponin T (c TnT) in detecting early cardiac damage (Figure 3). (Tables 1–3).

Past studies have shown that both doxorubicin and mitoxantrone form cardiotoxic complexes with iron. ADR-925, the hydrolysis product of dexrazoxane as well as and other metal chelators effectively remove Fe(III) from its complex with doxorubicin and mitoxantrone, thus conferring its cardioprotective activity by preventing iron-based oxidative damage to myocytes and their mitochondria (Hasinoff et al., 2003). A training set of sera from SHR with overt cardiotoxicity (c TnT $\geq$0.15 ng/ml and histologic lesion scores $\geq$1.0) were compared to sera obtained from control SHR prior to treatment or following only 1–3 treatments with saline alone and whose cTnT = 0. Also included in training as a positive were rats with lower cTnT levels ($\geq$0.08 ng/ml) but also with mild apparent pathologic changes as determined by histologic lesion scoring. Testing of a model comprised of the intensities of ions defined at 5 m/z features (m/z = 810.33765, 981.8242, 1987.9727, 2013.5771, 10645.952) on 36 blinded samples (test set 1) generated a result in which 22/22 positives were

TABLE 1A.—Control samples.

Treatment	(cTnT) ng/ml	Histology Score	Prediction
Pre-Dose	0	0	Negative
Pre-Dose	0	0	Negative
Pre-Dose	0	0	Negative
Pre-Dose	0	0	Negative
Pre-Dose	0	0	Negative
Pre-Dose	0	0	Negative
Pre-Dose	0	0	Negative
Pre-Dose	0	0	Negative
Pre-Dose	0	0	Negative
Pre-Dose	0	0	Negative
Pre-Dose	0	0	Negative
Pre-Dose	0.05	0	Negative
Pre-Dose	0	0	Negative
Saline × 1	0	0	Negative
Saline × 1	0	0	Negative
Saline × 1	0	0	Negative
Saline × 1	0.01	0	Negative
Saline × 7 wks	0	0	Negative
Saline × 7 wks	0	0	Negative
Saline × 7 wks	0	0	Negative
Saline × 9 wks	0	- N/A -	Negative
Saline × 9 wks	0	- N/A -	Negative
Saline × 9 wks	0	- N/A -	Negative
Saline × 9 wks	0	- N/A -	Negative
Saline × 9 wks	0	- N/A -	Negative
Saline × 9 wks	0	- N/A -	Negative
Saline × 9 wks	0	- N/A -	Negative
Saline × 9 wks	0	- N/A -	Negative
Saline × 9 wks	0	- N/A -	Negative
Saline × 9 wks	0	0	Negative
Saline × 9 wks	0	0	Negative
Saline × 9 wks	0	0	Negative
Saline × 9 wks	0	- N/A -	Negative
Saline × 9 wks	0.05	- N/A -	Negative
Saline × 9 wks	0.02	0	Negative
Saline × 10wks	0	0	Negative
Saline × 10 wks	0	0	Positive
Saline × 10 wks	0	0	Positive
Saline × 10 wks	0	0	Negative
Saline × 10 wks	0	0	Positive
Saline × 10 wks	0	0	Positive
Saline × 10 wks	0	0	Positive
Saline × 10 wks	0	0	Positive
Saline × 10 wks	0	0	Positive
Saline × 10 wks	0.04	0	Positive
Saline × 10 wks	0.06	0	Positive
Saline × 10 wks	0.01	0	Negative
Saline × 10 wks	0.05	0	Positive
Saline × 10 wks	0.03	0	Positive
Saline × 10 wks	0.04	0	Positive
Saline × 12 wks	0.02	0	Negative
Saline × 12 wks	0.07	0	Negative
Saline × 12 wks	0.03	0	Negative
Saline × 12 wks	0.03	0	Negative
Saline × 12 wks	0.03	0	Negative
Saline × 12 wks	0.01	0	Negative
Saline × 12 wks	0	0	Negative
Saline × 12 wks	0	0	Negative
Saline × 12 wks	0	0	Negative
Saline × 12 wks	0	0	Negative
Saline × 12 wks	0	0	Negative

TABLE 1B.—Dexrazoxane treated.

Treatment	(cTnT) ng/ml	Histology Score	Prediction
DZR 25 mg/kg × 1	0	0	Negative
DZR 25 mg/kg × 1	0	0	Negative
DZR 25 mg/kg × 1	0	0	Negative
DZR 25 mg/kg × 1	0.02	0	Negative
DZR 25 mg/kg × 1	0.01	0	Positive
DZR 25 mg/kg × 1	0.02	0	Negative
DZR 25 mg/kg × 1	0.02	0	Negative
DZR 25 mg/kg/wk × 7 wks	0	0	Negative
DZR 25 mg/kg/wk × 7 wks	0	0	Negative
DZR 25 mg/kg/wk × 7 wks	0.02	0	Negative
DZR 25 mg/kg/wk × 9 wks	0	- N/A -	Negative
DZR 25 mg/kg/wk × 9 wks	0	- N/A -	Negative
DZR 25 mg/kg/wk × 9 wks	0	- N/A -	Negative
DZR 25 mg/kg/wk × 9 wks	0	- N/A -	Negative
DZR 25 mg/kg/wk × 9 wks	0	- N/A -	Negative
DZR 25 mg/kg/wk × 12 wks	0	0	Negative
DZR 25 mg/kg/wk × 12 wks	0.02	0	Negative
DZR 25 mg/kg/wk × 12 wks	0.07	0	Negative

TABLE 2A.—Doxorubicin treated.

Treatment	(cTnT) ng/ml	Histology Score	Prediction
DOX 1 mg/kg/wk × 10 wks	0.03	2.0	Positive
DOX 1 mg/kg/wk × 10 wks	0.06	1.5	Positive
DOX 1 mg/kg/wk × 10 wks	0.03	1.5	Positive
DOX 1 mg/kg/wk × 10 wks	0.03	2.0	Positive
DOX 1 mg/kg/wk × 10 wks	1.10	2.0	Positive
DOX 1 mg/kg/wk × 10 wks	0.51	1.5	Positive
DOX 1 mg/kg/wk × 10 wks	0.17	1.0	Positive
DOX 1 mg/kg/wk × 10 wks	0.27	1.5	Positive
DOX 1 mg/kg/wk × 10 wks	0.50	2.5	Positive
DOX 1 mg/kg/wk × 10 wks	0.08	1.0	Positive
DOX 1 mg/kg/wk × 10 wks	0.10	1.0	Positive
DOX 1 mg/kg/wk × 10 wks	0.40	2.0	Positive
DOX 1 mg/kg/wk × 10 wks	0.20	1.0	Positive
DOX 1 mg/kg/wk × 10 wks	0.18	1.5	Positive
DOX 1 mg/kg/wk × 9 wks	0.04	- N/A -	Positive
DOX 1 mg/kg/wk × 9 wks	0.03	- N/A -	Positive
DOX 1 mg/kg/wk × 9 wks	0.30	- N/A -	Positive
DOX 1 mg/kg/wk × 9 wks	0.14	- N/A -	Positive
DOX 1 mg/kg/wk × 9 wks	0.02	- N/A -	Positive
DOX 1 mg/kg/wk × 9 wks	0.00	- N/A -	Positive
DOX 1 mg/kg/wk × 9 wks	0.00	- N/A -	Positive
DOX 1 mg/kg/wk × 9 wks	0.23	3.0	Positive
DOX 1 mg/kg/wk × 9 wks	0.22	1.5	Positive
DOX 1 mg/kg/wk × 9 wks	0.42	2.5	Positive
DOX 1 mg/kg/wk × 9 wks	0.68	2.5	Positive
DOX 1 mg/kg/wk × 9 wks	0.83	2.5	Positive
DOX 1 mg/kg/wk + mAB × 9 wks	0.67	- N/A -	Positive
DOX 1 mg/kg/wk + mAB × 9 wks	0.73	- N/A -	Positive
DOX 1 mg/kg/wk × 7wks	0.15	1.5	Positive
DOX 1 mg/kg/wk × 7wks	0.12	2.5	Positive
DOX 1 mg/kg/wk × 7wks	0.04	1.5	Positive
DOX 1 mg/kg/wk × 7wks	0.06	1.0	Negative
DOX 3 mg/kg × 1	0.00	0	Negative
DOX 3 mg/kg × 1	0.00	0	Positive
DOX 3 mg/kg × 1	0.01	0	Positive
DOX 3 mg/kg × 1	0.04	0	Negative
DOX 3 mg/kg × 1	0.02	0	Negative
DOX 3 mg/kg × 1	0.00	0	Negative
DOX 3 mg/kg × 1	0.04	0	Negative
DOX 3 mg/kg × 1	0.05	0	Negative
DOX 3 mg/kg × 1	0.06	0	Negative

correctly classified (including all 5 rats whose serum cTnT was low (between 0.08 and 0.15 ng/ml)), and 14/14 negatives. Also evaluated in a separate blinded test set were serum from 43 rats (test set 2) that were expected to be classified as

TABLE 2B.—Dexrazoxane pretreated and doxorubicin treated.

Treatment	(cTnT) ng/ml	Histology Score	Prediction
DOX 1 mg/kg/wk + 25 mg/kg/wk × 12 wks	0.38	1.5	Positive
DOX 1 mg/kg/wk + 25 mg/kg/wk × 12 wks	0.10	1.5	Positive
DOX 1 mg/kg/wk + 25 mg/kg/wk × 9 wks	0.02	- N/A -	Positive
DOX 1 mg/kg/wk + 25 mg/kg/wk × 9 wks	0	- N/A -	Positive
DOX 1 mg/kg/wk + 25 mg/kg/wk × 9 wks	0	- N/A -	Positive
DOX 1 mg/kg/wk + 25 mg/kg/wk × 9 wks	0.07	- N/A -	Positive
DOX 1 mg/kg/wk + 25 mg/kg/wk × 9 wks	0.02	- N/A -	Positive
DOX 1 mg/kg/wk + 25 mg/kg/wk × 7 wks	0.07	1.0	Negative
DOX 1 mg/kg/wk + 25 mg/kg/wk × 7 wks	0.05	1.0	Positive
DOX 1 mg/kg/wk + 25 mg/kg/wk × 7 wks	0	1.0	Negative
DOX 1 mg/kg/wk + 25 mg/kg/wk × 7 wks	0	1.0	Negative
DOX 1 mg/kg + 25 mg/kg × 1 wk	0.02	0	Negative
DOX 1 mg/kg + 25 mg/kg × 1 wk	0	0	Negative
DOX 1 mg/kg + 25 mg/kg × 1 wk	0.03	0	Negative
DOX 1 mg/kg + 25 mg/kg × 1 wk	0.02	0	Positive
DOX 1 mg/kg + 25 mg/kg × 1 wk	0.05	0	Negative
DOX 1 mg/kg + 25 mg/kg × 1 wk	0.01	0	Negative
DOX 1 mg/kg + 25 mg/kg × 1 wk	0.02	0	Positive
DOX 1 mg/kg + 25 mg/kg × 1 wk	0	0	Negative
DOX 1 mg/kg + 25 mg/kg × 1 wk	0	0	Negative
DOX 1 mg/kg + 25 mg/kg × 1 wk	0.03	0	Negative

TABLE 3A.—Mitoxantrone treated.

Treatment	(cTnT) ng/ml	Histology Score	Prediction
MTX 0.5 mg/kg/wk × 12 wks	0.11	2.0	Positive
MTX 0.5 mg/kg/wk × 12 wks	0.04	2.0	Positive
MTX 0.5 mg/kg/wk × 9 wks	0.03	- N/A -	Positive
MTX 0.5 mg/kg/wk × 9 wks	0	- N/A -	Positive
MTX 0.5 mg/kg/wk × 9 wks	0	- N/A -	Positive
MTX 0.5 mg/kg/wk × 9 wks	0	- N/A -	Positive
MTX 0.5 mg/kg/wk × 9 wks	0	- N/A -	Positive

negatives (histologic score = 0 or not taken) but were older as they were on long-term (6-to 12-week dosing) saline alone or dexrazoxane.

Because the animals were older and SHR develop hypertension and myopathy as they age, they had been excluded from the training set as definite negatives. The pattern was able to classify 35/43 (81%) correctly. Analysis of how the model performed on a further testing challenge set of 88 blinded "unknown" samples (test set 3) yielded a positive cardiotoxicity classification for 36 of the samples and 52 negative determinations. Importantly, 51/52 (98%) negatives were derived from rats that were pretreated with saline only, dexrazoxane alone, or doses of dexrazoxane prior to doxorubicin or mitoxantrone and could be expected to be considered truly negative by histopathology or only slight or no serum cardiac troponin T elevations (≤0.07 ng/ml).

Of the 36 classified positives in the last test set, 25 would be expected to be truly positive as they were treated with doxorubicin or mitoxantrone for 7 or more cycles, with the other 11 expected to be negative as they received saline or cardioprotectant alone. Interestingly, tabulating samples across all of the test sets, at the 7 week time point, 75% (3 of 4) of the animals dosed with the cardioprotectant before each dose of doxorubicin were classified as negative, but all animals (8 of 8) dosed for 9 weeks with both cardioprotectant and doxorubicin were classified as positive, reflecting the detectable breakthrough of toxicity as the protecting effects of pretreatment dosing were overcome. It is worth further emphasis that all of the study animals dosed with the less cardiotoxic anthracenedione mitoxantrone for 12 weeks were classified as diseased, even though

TABLE 3B.—Dexrazoxane pretreated and mitoxantrone treated.

Treatment	(cTnT) ng/ml	Histology Score	Prediction
MTX 0.5 mg/kg/wk + DZR 25 mg/kg/wk × 12 wks	0.04	1.0	Negative
MTX 0.5 mg/kg/wk + DZR 25 mg/kg/wk × 12 wks	0.05	1.5	Negative
MTX 0.5 mg/kg/wk + DZR 25 mg/kg/wk × 12 wks	0.04	1.0	Negative
MTX 0.5 mg/kg/wk + DZR 25 mg/kg/wk × 12 wks	0.04	1.5	Negative
MTX 0.5 mg/kg/wk + DZR 25 mg/kg/wk × 9 wks	0.03	- N/A -	Negative
MTX 0.5 mg/kg/wk + DZR 25 mg/kg/wk × 9 wks	0	- N/A -	Positive
MTX 0.5 mg/kg/wk + DZR 25 mg/kg/wk × 9 wks	0	- N/A -	Negative
MTX 0.5 mg/kg/wk + DZR 25 mg/kg/wk × 9 wks	0	- N/A -	Negative
MTX 0.5 mg/kg/wk + DZR 25 mg/kg/wk × 9 wks	0.02	- N/A -	Negative

no training set samples contained mitoxantrone treated rat serum. Note also that all animals predosed with cardioprotectant prior to mitoxantrone dosing for 12 weeks were recognized as negative, again distinguishing a boundary between toxicity and cardiotoxicity established by cardioprotectant pretreatment.

These results indicate that a serum proteomic pattern has classification accuracy that reflects quite well either the treatment history, serum c TnT levels, or the underlying histology of the heart damage that has occurred. Ongoing studies are being performed to determine if this pattern can detect an earlier onset of cardiotoxicity before troponin levels rise, and thus perhaps before irreversible and progressive heart damage has occurred. These spectra are posted at: ⟨http://clinicalproteomics.steem.com/⟩.

TOXICOPROTEOMICS: A VIEW TO THE FUTURE

Toxicoproteomics using proteomic pattern technology can have important direct applications within the drug development pipeline as well as potentially powerful bedside applications. Incorporation of high throughput screening of conditioned media, body fluids from animals into hit-to-lead screening, lead screening and preclinical validation may be possible. We can envision a future in which the specific serum/urine/plasma mass spectral proteomic portraits of a variety of major organ toxicities such as hepatotoxicity, nephrotoxicity, cardiotoxicity, and reprotoxicity, are used to rapidly screen against experimental compounds either for toxic liability or for protective intervention efficacy. In the future, the physician scientist and pathologist will use these different proteomic analyses at many points of disease management. Cross-species analysis can be performed where serum proteomic signatures of cardiotoxicity in rat, dog, and human can be concomitantly compared with each other to find those toxicity related signatures, which transcend across species.

This shifts even more importance to early preclinical animal based studies where a surrogate biomarker pattern, known to be predictive of the toxicity or protective efficacy in humans, can be used with more confidence as an early screening tool. Moreover, direct bedside monitoring of the patient's proteomic patterns can be performed during the clinical trials themselves. Diagnosis based on proteomic signatures can be a complement to histopathology; and perhaps even one day be used for individualized selection of therapeutic combinations that best target the patient's disease to provide the best therapeutic index. Mass spectroscopy analysis of the low

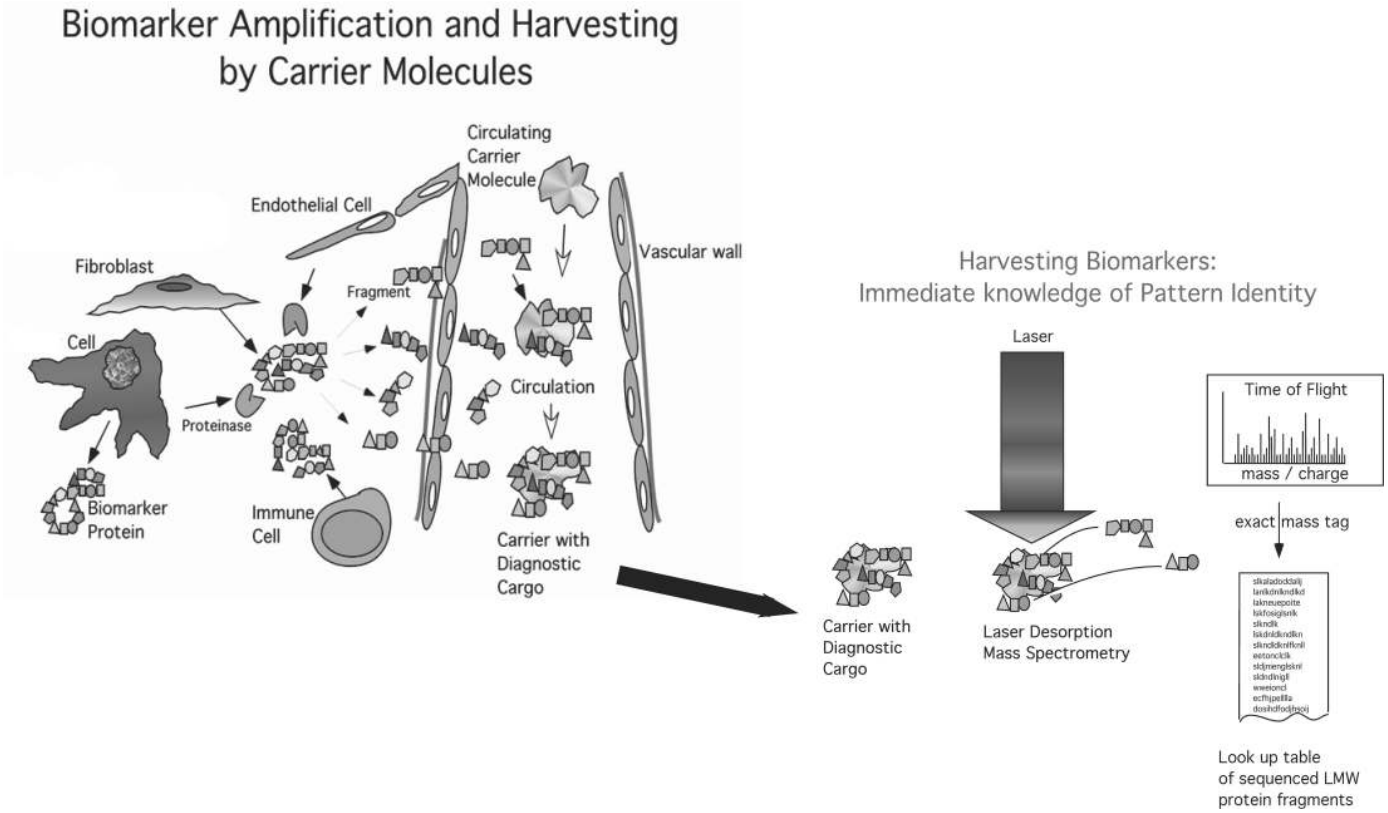

FIGURE 4.—Biomarker amplification and harvesting by carrier molecules. Low molecular weight peptide fragments, produced within the unique tissue microenvironment and generated as a consequence of the organ toxicity permeate through the endothelial cell wall barrier and trickle into the circulation. Here, these fragments are immediately are bound with circulating high abundance carrier proteins such as albumin and protected from kidney clearance. The resultant amplification of the biomarker fragments enables the ability to see these low abundance entities by mass spectrometry based detection and profiling. In the future, harvesting nanoparticles, engineered with high affinity for binding, can be distilled into the collected body fluids or injected directly into the circulation to bind with disease and toxicity related information archive. These nanoparticles and their bound diagnostic cargo can then be directly collected, filtered over engineered filters and queried by high-resolution mass spectrometry. A look up table, where the exact identities of each of the peaks will be compared against the accurate mass tag of each of the peaks within the spectra will enable the simultaneous identification of each entity within the pattern as well as the discovery of the diagnostic pattern itself.

molecular weight range of the serum/plasma proteome is a rapidly emerging frontier for biomarker discovery and clinical diagnostics. Since we now know that the vast majority of these biomarkers exist in association with circulating high molecular mass carrier proteins, these findings shift the focus of biomarker analysis to the carrier protein and its biomarker content.

Past conventional protocols for biomarker discovery discard the abundant "contaminating" high molecular mass proteins, in order to focus on the low mass range. Unfortunately this procedure removes most of the important diagnostic biomarkers. We can now develop new tools, created at the intersection of proteomics and nanotechnology whereby nanoharvesting agents can be instilled into the circulation (e.g., derivatized gold particles) or into the blood collection device to act as "molecular mops" that soak up and amplify the biomarkers that exist (8) (Figure 4). These nanoparticles, with their bound diagnostic cargo, can be directly queried via mass spectrometry and the low molecular weight and enriched biomarker signatures revealed.

REFERENCES

Adam, B. L., Qu, Y., Davis, J. W., Ward, M. D., Clements, M. A., Cazares, L. H., Semmes, O. J., Schellhammer, P. F., Yasui, Y., Feng, Z., and Wright, Jr. G. L. (2002). Serum protein fingerprinting coupled with a pattern-matching algorithm distinguishes prostate cancer from benign prostate hyperplasia and healthy men. *Cancer Res* **62**(13), 3609–14.

Alderton, P. M., Gross, J., and Green, M. D. (XXX). Comparative study of doxorubicin, mitoxantrone, and epirubicin in combination with ICRF-187 (ADR-529). *Am J Pathol* **14**(2), 1916–26.

Anderson, N. L., and Anderson, N. G. (2002). The human plasma proteome: history, character, and diagnostic prospects. *Mol Cell Proteomics* **11**, 845–67.

Bristow, M. R., Mason, J. W., Billingham, M. E., et al. (1981). Dose-effect and structure-function relationships in doxorubicin cardiomyopathy. *Am Heart J* **102**, 709–18.

Cojocel, C., Maita, K., Baumann, K., and Hook, J. B. (1984). Renal processing of low molecular weight proteins. *Pflugers Arch* **401**(4), 333–9.

Conrads, T. P., Zhou, M., Petricoin, E. F. III, Liotta, L., and Veenstra, T. D. (2003). Cancer diagnosis using proteomic patterns. *Expert Rev Mol Diagn* **3**(4), 411–20.

Ewer, M. S., Gibbs, H. R., Swafford, J., et al. (1999). Cardiotoxicity in patients receiving transtuzumab (Herceptin): primary toxicity, synergistic or sequential stress, or surveillance artifact? *Semin Oncol* **26**(suppl. 12), 96–101.

Hasinoff, B. B., Hellmann, K., Herman, E. H., and Ferrans, V. J. (1998). Chemical, biological and clinical aspects of dexrazoxane and other bisdioxopiperazines. *Curr Med Chem* **5**(1), 1–28.

Hasinoff, B. B., Schnabl, K. L., Marusak, R. A., Patel, D., and Huebner, E. (2003). Dexrazoxane (ICRF-187) protects cardiac myocytes against doxorubicin by preventing damage to mitochondria. *Cardiovasc Toxicol* **3**(2), 89–99.

Herman, E. H., and Ferrans, V. J. (1998). Preclinical animal models of cardiac protection from anthracycline-induced cardiotoxicity. *Semin Oncol* **25**(Suppl 10), 15–21.

Herman, E. H., Zhang, J., Rifai, N., Lipshultz, S. E., Hasinoff, B. B., Chadwick, D. P., Knapton, A., Chai, J., and Ferrans, V. J. (2001). The use of serum levels of cardiac troponin T to compare the protective activity of dexrazoxane against doxorubicin- and mitoxantrone-induced cardiotoxicity. *Cancer Chemother Pharmacol* **48**(4), 297–304.

Hingorani, S. R., Emanuel, F., Petricoin, E. F., III, Maitra, A., Rajapakse, V., King, C., Jacobetz, M. A., Ross, S., Conrads, T. P., Veenstra, T. D., Hitt, B. A., Kawaguchi, Y., Zhou, Y., Johann, D., Liotta, L. A., Crawford, H. C., Putt, M. E., Jacks, T., Konieczny, S. F., Wright, C. E., Hruban, R. E., Lowry, A. M., and Tuveson D. A. (2003). Preinvasive and invasive ductal pancreatic cancer and its early detection in the mouse. *Cancer Cell* **10**, 6–21.

Holland, J. H., ed. (1994). *Adaptation in Natural and Artificial Systems: an Introductory Analysis with Applications to Biology, Control, and Artificial Intelligence*, 3rd ed., MIT Press Cambridge, Massachusetts.

Kantor, A. B. (2002). Comprehensive phenotyping and biological marker discovery. *Dis Markers* **18**(2), 91–7.

Kohonen, T. (1982). Self-organizing formation of topologically correct feature maps. *Biol Cybernetics* **43**, 59–69.

Kohonen, T. (1990). The self-organizing map. *Proc IEEE* **78**, 1464–80.

Lambertenghi-Deliliers G., Zanon, P. L., Pozzoli, E. F., et al. (1976) Myocardial injury induced by a single dose of adriamycin: an electron microscopic study. *Tumor* **62**, 517–28.

Li, J., Zhang, Z., Rosenzweig, J., Wang, Y. Y., and Chan, D. W. (2002). Proteomics and bioinformatics approaches for identification of serum biomarkers to detect breast cancer. *Clin Chem* **48**(8), 1296–304.

Liotta, L. A., Ferrari, M., and Petricoin, E. (2003). Clinical proteomics: written in blood. *Nature* **425**, 905.

Maack, T. (1975). Renal handling of low molecular weight proteins. *Am J Med* **58**(1), 57–64.

McDonald, W. H., and Yates, J. R., III. (2002). Shotgun proteomics and biomarker discovery. *Dis Markers* **18**(2), 99–105.

Mehta, A., Ross, S., Lowenthal, M. S., Fusaro, V. Fishman, D. A., Petricoin, E. F., and Liotta, L. A. (2003). Biomarker amplification by serum carrier protein binding. *Disease Markers* **19**, 1–10.

Petricoin, E. F., III, Ardekani, A. M., Hitt, B. A., Levine, P. J., Fusaro, V. A., Steinberg, S. M., Mills, G. B., Simone, C., Fishman, D. A., Kohn, E. C., and Liotta, L. A. (2002a). Use of proteomic patterns in serum to identify ovarian cancer. *Lancet* **359**(9306), 572–7.

Petricoin, E., III, and Liotta, L. A. (2003a). Counterpoint: the vision for a new diagnostic paradigm. *Clin Chem* **49**(8):

Petricoin, E. F., and Liotta, L. A. (2003b). Mass spectrometry-based diagnostics: the upcoming revolution in disease detection. *Clin Chem* **49**(4), 533–4.

Petricoin, E. F., III, Mills, G. B., Kohn, E. S., Liotta, L. A. (2002b). Proteomic patterns in serum and identification of ovarian cancer [Reply]. *Lancet* **360**, 170–1.

Petricoin, E. F., III, Ornstein, D. K., Paweletz, C. P., Ardekani, A., Hackett, P. S., Hitt, B. A., Velassco, A., Trucco, C., Wiegand, L., Wood, K., Simone, C. B., Levine, P. J., Linehan, W. M., Emmert-Buck, M. R., Steinberg, S. M., Kohn, E. C., and Liotta, L. A. (2002c). Serum proteomic patterns for detection of prostate cancer. *J Natl Cancer Inst* **94**(20), 1576–8.

Tirumalai, R. S., Chan, K. C., Prieto, D. A., Issaq, H. J., Conrads, T. P., and Veenstra, T. D. (2003). Characterization of the low molecular weight human serum proteome. *Mol Cell Proteomics* **2**(10), 1096–103. [Epub 2003 Aug 13].

Tou, J. T., and Gonzalez, R., eds. (1974). Pattern Classification by Distance Functions. In *Pattern Recognition Principles*, Reodina MA: Addison Weley Publishing Comapny. New York.

Ward, J. B. Jr., and Henderson, R. E. (1996). Identification of needs in biomarker research. *Environ Health Perspect* **104**(Suppl. 5), 895–900.

Zhang, J., Herman, E. H., and Ferrans, V. J. (1993). Dendritic cells in the hearts of spontaneously hypertensive rats treated with doxorubicin with or without ICRF-187. *Am J Pathol* **142**(6), 1916–26.

Zhang, J., Herman, E. H., Knapton, A., Chadwick, D. P., Whitehurst, V. E., Koerner, J. E., Papoian, T., Ferrans, V. J., and Sistare, F. D. (2002). SK&F 95654-Induced acute cardiovascular toxicity in Sprague-Dawley rats—histopathologic, electron microscopic, and immunohistochemical studies. *Toxicol Pathol* **30**(1), 28–40.